

Formation of ZnSe Nanoclusters in Silicon Dioxide Layers by High-Fluence Ion Implantation: Experimental Data and Simulation Results

M.A. MAKHAVIKOU^a, F.F. KOMAROV^{a,*}, A.F. KOMAROV^a,
S.A. MISKIEWICZ^a, O.V. MILCHANIN^a, L.A. VLASUKOVA^b,
I.N. PARKHOMENKO^b, J. ŽUK^c AND E. WENDLER^d

^a*Institute of Applied Physics Problems, Kurchatov Street 7, 220045 Minsk, Belarus*

^b*Belarusian State University, Independence Ave. 4, 220030 Minsk, Belarus*

^c*Maria Curie-Skłodowska University, Pl. M. Curie-Skłodowskiej 1, 20-031 Lublin, Poland*

^d*Friedrich Schiller University Jena, Max-Wien-Platz 1, D-07743 Jena, Germany*

Doi: [10.12693/APhysPolA.142.684](https://doi.org/10.12693/APhysPolA.142.684)

*e-mail: komarovf@bsu.by

The synthesis of ZnSe nanoclusters produced by high-fluence implantation of Zn⁺ and Se⁺ ions into silica is numerically simulated. The developed model is based on solving the system of the convection–diffusion–reaction equations. The ion-beam synthesized nanoclusters were identified using the transmission electron diffraction method as ZnSe nanocrystals. According to the transmission electron microscopy data, the nanocrystal density amounts to $1.15 \times 10^{12} \text{ cm}^{-2}$, and the mean diameter is 5 nm. The fraction of the total number of implanted Se atoms bound with Zn during the formation of ZnSe nanocrystals was counted from the transmission electron microscopy images. It amounts to $\sim 5.6 \text{ at.}\%$. This value was used to calculate the mean values of the radiation-enhanced diffusion coefficients in the silica. For Zn atoms $D_{\text{Zn}} = 1.94 \times 10^{-16} \text{ cm}^2/\text{s}$, and for Se atoms $D_{\text{Se}} = 2.88 \times 10^{-16} \text{ cm}^2/\text{s}$. A comparison of simulation results with experimental data revealed a reasonable correlation.

topics: silica, ion-beam synthesized ZnSe nanocrystals, transmission electron microscopy, Rutherford backscattering spectroscopy

1. Introduction

Silicon is the basic material of modern microelectronics, which can be used to manufacture almost all types of electronic devices. However, it is not effective in optoelectronics due to the indirect band gap and low interband emissivity. The progress of silicon optoelectronics is related to the adaptation of semiconductor materials with improved optical characteristics to the existing Si technology. For this purpose, compounds A²B⁶, e.g., ZnSe, can be perspective materials. ZnSe has unique optical and electrical properties such as a wide direct band gap (2.7 eV), large exciton binding energy (21 meV), high refractive index, large photoresistivity, non-toxicity, low absorptivity in the infrared (IR) and visible spectral range [1]. Due to these valuable properties, ZnSe is used as a basis in many types of devices, e.g., RGB laser diodes [2], sensors [3], nonlinear optical devices [4], laser screens, and thin film transistors [5].

Modern methods of synthesis of A²B⁶ nanostructures include molecular beam epitaxy [6], magnetron sputtering [7], sol–gel method [8], chemical deposition [9, 10], and high-fluence ion

implantation [11, 12]. The last one is the most preferred due to its full compatibility with existing silicon technology.

The formation of impurity profiles during the implantation of high-fluence ion ($D > 10^{16} \text{ ion}/\text{cm}^2$) depends on a number of characteristics: kinetics of atomic collisions, accumulation of impurity in the target, sputtering and swelling of the target surface, diffusion of impurity, formation of new phases during implantation [13]. Thus, the existing models of the embedded impurity distribution [14, 15] and diffusion-kinetic parameters [16, 17] should be adapted to certain implantation regimes, target types, as well as physical and chemical characteristics of the target and impurity. Simulation of the formation of nanoclusters during the high-fluence ion implantation should be considered as a number of tasks [18–21]: the processes of irradiation of the target with high ion fluence, calculation of the fraction of implanted atom forming nanoclusters, finding the regularity of nucleation and the new phase cluster growth, as well as the control of the size distribution and evolution of nanoclusters during ion implantation and thermal processing.

Cluster formation due to precipitation or Ostwald growth is described by a Gauss size distribution [22]. However, the system does not keep the initial size distribution of clusters during long-term high-fluence implantation or thermal processing. In this case, it is necessary to modify the Gauss size cluster distribution [23] in order to achieve the coincidence of the simulation results with the experimental data [24]. The form of the size distribution depends on the diffusion mobility of atoms during implantation, the impurity solubility, and the ion bulk flow [18].

The issue of ion-beam synthesis of ZnSe nanocrystals in silica layers on silicon was discussed in our previous papers [25, 26]. It was shown that it is possible to obtain ZnSe/SiO₂ nanocomposites with improved structure and optical properties via high-fluence “hot” ion implantation (500°C) of Zn and Se into a silica matrix. However, the simulation of high-fluence implantation of Zn and Se to silica, as well as the mechanisms of ZnSe nanocluster formation, were not considered. Calculations, as well as a physical–mathematical model of high-fluence implantation of As and In in Si, were provided in [27]. The authors took into account radiation-enhanced diffusion of impurity, sputtering and swelling of the target, and formation of a new phase. The purpose of the present paper is to adjust the model from [27] to the ion implantation of Zn and Se into the silica matrix and to compare the simulation results with experimentally obtained data on the structural and phase composition of ZnSe/SiO₂ nanocomposites.

2. Materials and methods

The initial SiO₂ (600 nm)/Si samples (2 × 2 cm²) were cut from the thermally oxidized Si substrates. These samples were implanted at first with 150 keV Zn ions and then with 170 keV Se ions to the same fluence of 4 × 10¹⁶ ions/cm² at 550°C. Based on SRIM calculations [28], implantation energies of 150 keV for the Zn⁺ ions and 170 keV for the Se⁺ ions were chosen to obtain nearly the same mean projected range for both species in silica. After the implantation procedure, the samples were not subjected to any additional annealing.

The concentration of Zn and Se atoms versus depth for the implanted and annealed samples was obtained by Rutherford backscattering spectroscopy (RBS) using 2 MeV He⁺ ions. The Zn and Se distributions were extracted by fitting the calculated RBS spectra to the experimental spectra using the SIMNRA code [29]. For the sake of comparison, the Zn and Se depth profiles were calculated using SRIM-2010 [28]. The structural and phase composition of the as-implanted samples was examined by transmission electron microscopy (TEM) with a Hitachi H-800 200 keV transmission electron microscope in the plan-view geometry and selected area electron diffraction (SAED).

3. Model

The results of experimental investigations of the structural-phase composition of the ZnSe/SiO₂ nanocomposite were reported in detail earlier in our papers [25, 26]. These experimental data were used for comparison with the calculation results obtained in the present investigations. The TEM data, diffraction pattern, and size distribution of clusters in the silica sample implanted with Zn and Se are shown in Fig. 1. Hot implantation of high-fluences of Zn and Se results in the formation of clusters with an average size of 5 nm. The appearance of three concentric rings of planes {111}, {220}, and {311} (inset in Fig. 1a) confirms the crystal structure of ZnSe nanoclusters.

The density, size distribution, and fraction of the total number of implanted Se atoms bound with Zn during the formation of ZnSe nanocrystals were calculated (Table I). The Se fraction bound with Zn in the ZnSe nanocrystals amounts to ~ 5.6 at.%. It should be noted that the TEM resolution is ~ 1 nm, and clusters of smaller sizes were not counted. One can suggest that the real Se fraction bound in the ZnSe crystallites should be more significant.

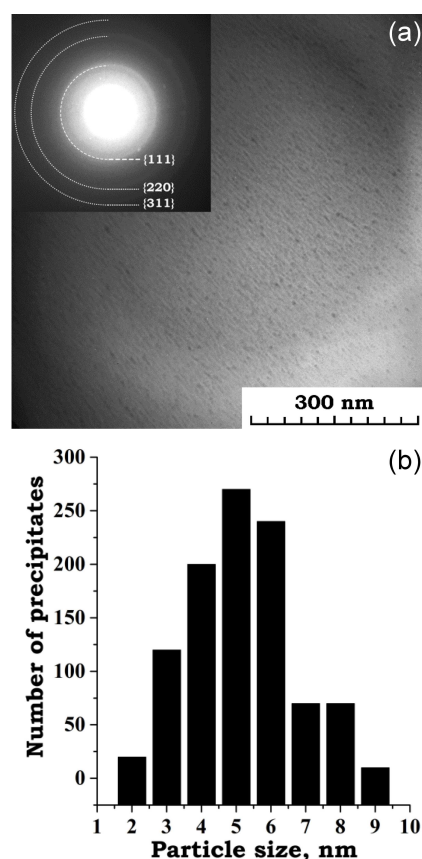


Fig. 1. Bright-field TEM-image in the “plan-view” of SiO₂ layers after hot implantation of a silica sample with Zn and Se (a) and size distribution of ZnSe nanocrystals (b). The insert shows the electron diffraction pattern from ZnSe nanocrystals.

TABLE I

Number of counted ZnSe nanocrystals, their density and average size, and a fraction of Se atoms bound with Zn in the ZnSe nanocrystals.

Implantation regime	Counted number of ZnSe nanoclusters	Density of ZnSe nanoclusters [cm ⁻²]	Average size of nanoclusters [nm]	Se fraction in ZnSe nanoclusters [%]
Zn (150 keV, 4 × 10 ¹⁶) Se (170 keV, 4 × 10 ¹⁶) Implantation at 550°C	1000	1.145 × 10 ¹²	5 ± 1	5.6

A model of calculation of concentration profiles for impurity distribution during high-fluence ion implantation was developed. The formation of implantation profiles is determined by the following processes: accumulation of implanted impurity in the target, sputtering of the target surface, diffusion of impurity atoms, formation of new phases during implantation, and radiation swelling due to material density change.

Corresponding to experimental studies, first of all, ion implantation of Zn (150 keV, 4 × 10¹⁶ cm⁻²) and then Se (170 keV, 4 × 10¹⁶ cm⁻²) at $t = 550^\circ\text{C}$ in silica should be simulated. The flow of Zn atoms in silica is described by the formula

$$j_{\text{Zn}}(z, t) = -G_{\text{Zn}}N_{\text{Zn}}(z, t) - D_{\text{Zn}}(z, t)\frac{\partial N_{\text{Zn}}(z, t)}{\partial z}, \quad (1)$$

where $N_{\text{Zn}}(z, t)$ is the concentration of Zn depending on time t and depth z ; $G_{\text{Zn}}(z, t)$ is the local migration rate of Zn atom at time t and depth z due to the target sputtering and swelling as well as diffusion redistribution; $D_{\text{Zn}}(z, t)$ is the diffusion coefficient of Zn depending on depth and time due to the change of the irradiated layer characteristics after high-fluence implantation of impurity atoms.

The model of radiation-stimulated diffusion takes into account the dependence of the impurity diffusion coefficient on the depth distribution of the defects $F_d(z)$ [13], accordingly

$$D_{\text{Zn}}(z, t) = k \Phi(t) F_d(z), \quad (2)$$

where k is the proportionality factor (fitting parameter); $\Phi(t)$ is the fluence dependent on the irradiation time t ; $F_d(z)$ is the average energy released in the volume element as a result of the elastic impacts of the incident ions and all formed recoil atoms with the target atoms.

The local rate of sputtering- and swelling-induced Zn atom migration entering into (1) has the form [30]

$$G_{\text{Zn}}(z, t) = J_{\text{Zn}} Y(t) - V_{\text{Zn}}^i \int dz \frac{\partial N_{\text{Zn}}(z, t)}{\partial t}, \quad (3)$$

where J_{Zn} is the ion current density; $Y(t)$ is a function describing the sputtering that depends on the properties of the target surface; V_{Zn}^i is the volume of the implanted atom.

According to the conservation law, the equation of the Zn implantation process is as follows

$$\frac{\partial N_{\text{Zn}}(z, t)}{\partial t} = -\frac{\partial j_{\text{Zn}}}{\partial z} + f_{\text{Zn}}^i(z, t), \quad (4)$$

where $f_{\text{Zn}}^i(z, t)$ is a function of the source of unbound Zn atoms (not chemically bound with Se).

Thus, the final equation of the implantation of a high-fluence Zn ions in SiO₂ is described as

$$\frac{\partial N_{\text{Zn}}(z, t)}{\partial t} = \frac{\partial}{\partial z} \left[G_{\text{Zn}}(z, t) N_{\text{Zn}}(z, t) + D_{\text{Zn}}(z, t) \frac{\partial N_{\text{Zn}}(z, t)}{\partial z} \right] + f_{\text{Zn}}^i(z, t). \quad (5)$$

The model of Se implantation in SiO₂ is presented below.

According to experimental data confirmed by SAED and RBS, ZnSe nanocrystals were synthesized during implantation of high-fluence Zn and Se ions at $t = 550^\circ\text{C}$ in SiO₂. The flow of Se atoms bound with Zn and the flow of unbound Se atoms should be considered separately due to their different properties. The flow of chemically bound Se atoms during irradiation is caused by the radiation sputtering and swelling of the silica due to the continued implantation of impurity, but does not participate in the diffusion movement. Thus, the local movement speed $G_{\text{Se}}(z, t)$ of Se atoms bound with Zn atoms at time t and depth z is presented as

$$G_{\text{Se}}(z, t) = J_{\text{Se}}(z, t) Y(t)$$

$$-V_{\text{Se}}^i \int_0^z dz' \frac{\partial}{\partial t} \left[N_{\text{Se}}(z', t) + n_{\text{Se}}(z', t) \right], \quad (6)$$

where $N_{\text{Se}}(z, t)$ is the concentration of unbound Se atoms at the depth z and time t ; $n_{\text{Se}}(z, t)$ is the concentration of Se bound with Zn atoms at the time t and depth z .

According to the conservation law for Se atoms, the implantation equation of Se atoms is described as

$$\begin{aligned} \frac{\partial N_{\text{Se}}(z, t)}{\partial z} &= -\frac{dj_{\text{Se}}}{dz} + f_{\text{Se}}(z, t), \\ \frac{\partial n_{\text{Se}}(z, t)}{\partial t} &= -\frac{dj_{\text{Se}}}{dz} + f_{\text{Se}}^n(z, t), \\ f_{\text{Se}}(z, t) &= f_{\text{Se}}^i(z, t) - f_{\text{Se}}^\gamma(z, t), \end{aligned} \quad (7)$$

TABLE II

Simulation initial data.

Parameters	Zn	Se
Target atom concentration [atom/cm ²]	6.614 × 10 ²²	6.614 × 10 ²²
Ion energy E [keV]	150	170
Fluence Φ [ion/cm ²]	4 × 10 ¹⁶	4 × 10 ¹⁶
Ion current density J [μ A/cm ²]	2–3	2–3
Projective range of ion R_p [nm]	78.93	67.79
Lengthwise straggling ΔR_p [nm]	26.21	24.11
Profile asymmetry S_k	0.234	0.288
Energy released during elastic collisions $\nu(E)$ [keV]	51.29	58.43
Average depth of spatial distribution of energy released during elastic collisions R_{pd} [nm]	40.53	36.00
Lengthwise straggling of spatial distribution of energy released during elastic collisions ΔR_{pd} [nm]	27.60	24.32
Asymmetry of depth distribution profile of energy released during elastic collisions S_{kd}	0.74	0.75
Target sputtering coefficient S	2.12	2.50
Movement speed of impurity through target surface K^s [cm/s]	1.5 × 10 ⁻⁸	1.3 × 10 ⁻⁸
Coefficient of ZnSe phase formation speed K^γ [cm ³ /s]	1.5 × 10 ⁻²⁴	
Diffusion coefficient [cm ² /s]	1.94 × 10 ⁻¹⁶	2.88 × 10 ⁻¹⁶

where $f_{\text{Se}}^n(z, t)$ is a function of the source of the bound atoms; $f_{\text{Se}}^\gamma(z, t)$ is a function equal to the number of Se atoms bound with the previously implanted Zn atoms at time t and depth z . According to the theory of chemical reactions, the function $f_{\text{Se}}^\gamma(z, t)$ is proportional to the product of concentrations of reactive components given as

$$f_{\text{Se}}^\gamma(z, t) = K^\gamma N_{\text{Zn}}^t(z, t=\text{const}) N_{\text{Se}}(z, t), \quad (8)$$

where $N_{\text{Zn}}^t(z, t)$ is the concentration of Zn not chemically bound with Se; K^γ is the speed factor of the ZnSe nanocrystals formation, which depends on the properties of the impurity and target, temperature, type, and concentration of defects formed during ion implantation.

The function of bound atoms source in (7) is as follows

$$f_{\text{Se}}^n(z, t) = f_{\text{Se}}^\gamma(z, t). \quad (9)$$

The IV-type Pearson distribution $F_P(z)$ was chosen as a function of the distribution of the stopped ions at depth z and time t for both Zn (f_{Zn}^i) and Se atoms (f_{Se}^i) [27], thus

$$f_{\text{Zn,Se}}^i = J_{\text{Zn,Se}} F_P(z). \quad (10)$$

The system of two equations describing the high-fluence ion implantation of Se in SiO₂ lattice previously Zn-implanted at high temperature is as follows

$$\begin{aligned} \frac{\partial N_{\text{Se}}(z, t)}{\partial t} &= \frac{\partial}{\partial z} \left[G_{\text{Se}}(z, t) N_{\text{Se}}(z, t) \right. \\ &\left. + D_{\text{Se}}(z, t) \frac{\partial N_{\text{Se}}(z, t)}{\partial t} \right] + f_{\text{Se}}^i(z, t) - f_{\text{Se}}^\gamma(z, t), \end{aligned} \quad (11)$$

$$\frac{\partial n_{\text{Se}}(z, t)}{\partial t} = \frac{\partial}{\partial z} \left[G_{\text{Se}}(z, t) n_{\text{Se}}(z, t) \right] + f_{\text{Se}}^\gamma(z, t). \quad (12)$$

Now, (5), (11), and (12) are the system of equations of convection, diffusion, and reaction [27], respectively. The mathematical model of the implantation of Zn and Se ions in SiO₂ is based on the solution of the nonlinear diffusion–kinetic equations (5), (11), and (12).

The initial and boundary conditions for a semi-infinite target are respectively

$$\begin{aligned} N_{\text{Zn}}(z, t=0) &= 0, & n_{\text{Se}}(z, t=0) &= N_{\text{Se}}(z, t=0) = 0, \\ N_{\text{Zn}}(\infty, t) &= 0, & n_{\text{Se}}(\infty, t) &= N_{\text{Se}}(\infty, t) = 0. \end{aligned} \quad (13)$$

The diffusion of impurity atoms through the target surface is taken into account in the boundary condition

$$D_{\text{Zn,Se}} \frac{\partial N_{\text{Zn,Se}}(0, t)}{\partial z} = K_{\text{Zn,Se}}^s N_{\text{Zn,Se}}(0, t), \quad (14)$$

where $K_{\text{Zn,Se}}^s$ is the movement speed of impurity (Zn or Se) through the target surface. This factor is selected according to the correspondence of the calculated and experimental impurity concentration profiles. It is assumed that bound impurities do not participate in diffusion.

Initial data of the model for calculating the concentration profiles of implanted Zn and Se in the SiO₂ lattice are given in Table II.

In Table II, E , J , and Φ indicate the implantation regimes of Se and Zn ions in the silica lattice; R_p , ΔR_p , S_k , R_{pd} , ΔR_{pd} , S_{kd} , and $\nu(E)$ are the spatial

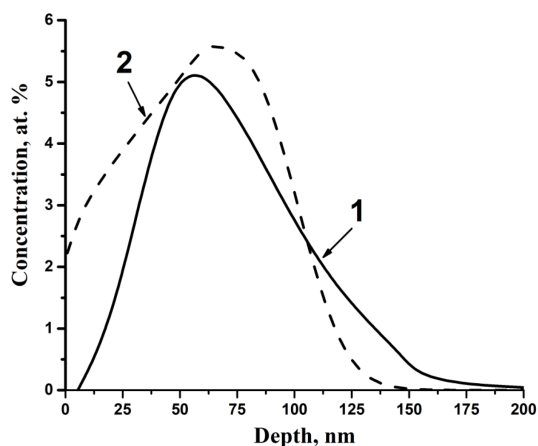


Fig. 2. Depth distribution of Zn in silica: 1 — experiment, 2 — calculation.

distribution moments of implanted atoms and the energy released during elastic collisions, calculated according to the inverse Boltzmann kinetic equation [13]. The coefficient of target sputtering of Zn and Se ions is calculated in the frame of the TRIM code [24].

4. Results and discussion

Calculated and experimental profiles of the depth distribution of implanted Zn ($E = 150$ keV, fluence $D = 4 \times 10^{16}$ ion/cm²) in silica are shown in Fig. 2. The calculated profile differs significantly from the experimental one on the edges, while the maxima of the theoretical and experimental profiles practically coincide. The calculated diffusion coefficient of Zn for a given fluence is $D_{\text{Zn}} = 1.94 \times 10^{-16}$ cm²/s. The difference between the calculated and experimental distribution profiles of Zn atoms in the silica lattice can be explained by the complex dependence of the diffusion coefficient on ion fluence and the function of defect depth distribution.

Calculated and experimental profiles of implanted Se ($E = 170$ keV, $D = 4 \times 10^{16}$ ion/cm²) in the silica pre-implanted with Zn ($E = 150$ keV, $D = 4 \times 10^{16}$ ion/cm²) as well as the bright-field TEM image of the sample are shown in Fig. 3.

According to this experiment, a part of Se atoms (~ 5.6 at.%) after ion implantation is bound with the pre-implanted Zn, forming ZnSe nanocrystals [25]. The value ~ 5.6 at.% is used in (7)–(9) to calculate the depth profile of the Se distribution in silica. After solving these equations, we found the diffusion coefficient of Se in silica, i.e., $D_{\text{Se}} = 2.88 \times 10^{-16}$ cm²/s. The fraction of Se bound with Zn relative to the total Se concentration (curve 4) is shown in Fig. 3. The TEM image shows that the shape of the depth profile of the formed ZnSe nanocrystals density after ion implantation matches the calculated profile of Se atoms (~ 6.2 at.%) bound with Zn (curve 4 in Fig. 3a).

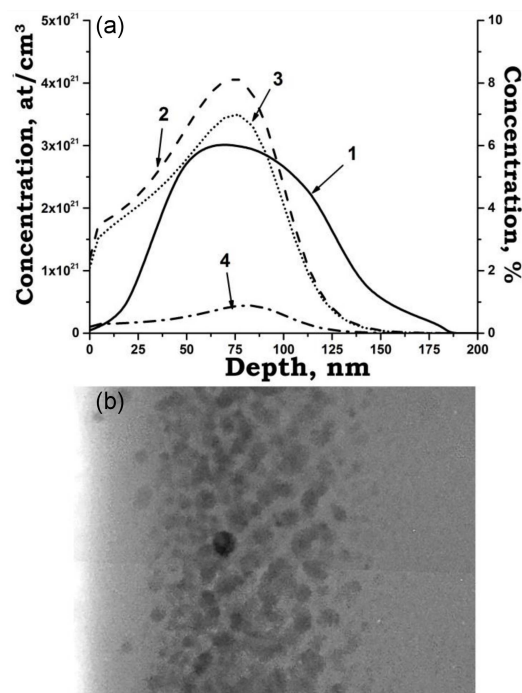


Fig. 3. Depth Se distribution in silica, (a) 1 — experiment; 2–4 — model: 2 — Se total concentration in silica, 3 — Se not bound with Zn, 4 — Se bound with Zn (ZnSe nanoclusters) and bright-field TEM-image in cross-section of SiO₂ layer with ZnSe nanoclusters (b) after hot implantation of a silica sample.

5. Conclusions

Using TEM and SAED, it was found that the implantation of Zn (150 keV, 4×10^{16} cm⁻²) and Se (170 keV, 4×10^{16} cm⁻²) into silica at 550°C leads to the formation of ZnSe nanocrystals, with the mean diameter of 5 nm which are distributed with the density of 1.15×10^{12} cm⁻².

The physical-mathematical model was developed to simulate the high-fluence implantation of zinc and selenium into silica. The model takes into account the processes of radiation-enhanced diffusion, sputtering and swelling of the target, and the formation of a new phase. The dependence of the diffusion coefficient on the depth distribution of defects entered into the silica target during Zn and Se implantation was also included in the model. In terms of the model, depth profiling of impurity (both in a free state and in the nanoclusters) was made.

Mean values of the radiation-enhanced diffusion coefficients for zinc ($D_{\text{Zn}} = 1.94 \times 10^{-16}$ cm²/s) and selenium ($D_{\text{Se}} = 2.88 \times 10^{-16}$ cm²/s) in silica were determined based on calculated and experimental data. The developed model gives the opportunity not only to find the mean coefficients of radiation-enhanced diffusion of impurities in silica, but also to determine the fraction of the bound Se impurity (6.2 at.%), i.e., the impurity entering into the ZnSe nanoclusters.

Acknowledgments

This study was supported by the Belarusian State Program of Scientific Research “Photonics and electronic for innovations” (Projects 3.8.1, SR No. 20212595 and 3.8.2, SR No. 20212655).

References

- [1] L. Zuala, P. Agarwal, *J. Mater. Sci. Mater. Electron.* **31**, 14756 (2020).
- [2] T.R. Kumar, P. Prabukanthan, G. Harichandran, J. Theerthagiri, A.M. Moydeen, G. Durai, P. Kuppusami, T. Tatarchuk, *J. Mater. Sci. Mater. Electron.* **29**, 5638 (2018).
- [3] U. Choudhari, S. Jagtap, *J. Electron. Mater.* **49**, 5903 (2020).
- [4] R. Šuminas, G. Tamošauskas, G. Valiulis, V. Jukna, A. Couairon, A. Dubietis, *Appl. Phys. Lett.* **110**, 241106 (2017).
- [5] D.D. Hile, H.C. Swart, S.V. Motloung, T.E. Motaung, L.F. Koao, *Phys. B: Phys. Condensed Matter* **575**, 411706 (2019).
- [6] Y.G. Sidorov, S.A. Dvoretiskii, V.S. Varavin, N.N. Mikhailov, M.V. Yakushev, I.V. Sabinina, *Semiconductors* **35**, 1045 (2001).
- [7] S.K. Mandal, S. Chaudhuri, A.K. Pal, *Thin Solid Films* **350**, 209 (1999).
- [8] B. Bhattacharjee, D. Ganguli, S. Chaudhuri, A.K. Pal, *Thin Solid Films* **422**, 98 (2002).
- [9] J.C. Sánchez-López, A. Fernández, *Thin Solid Films* **317**, 497 (1998).
- [10] J.F. Suyver, S.F. Wuister, J.J. Kelly, A. Meijerink, *Nano Lett.* **1**, 429 (2001).
- [11] A. Meldrum, E. Sonder, R.A. Zuhr, I.M. Anderson, J.D. Budai, C.W. White, L.A. Boatner, D.O. Henderson, *J. Mater. Res.* **14**, 4489 (1999).
- [12] K.Y. Gao, H. Karl, I. Grosshans, W. Hipp, B. Stritzker, *Nucl. Instrum. Methods Phys. Res. B* **196**, 68 (2002).
- [13] A.F. Burenkov, S.J. Anoretty, *Tables of Ion Implantation Spatial Distributions*, Gordon and Breach, New York 1986.
- [14] W. Möller, W. Eckstein, J.P. Biersack, *Comput. Phys. Commun.* **51**, 355 (1988).
- [15] A. Schonborn, N. Hecking, E.H. Kaat, *Nucl. Instrum. Methods Phys. Res. B* **43**, 170 (1989).
- [16] E.B. Boiko, F.F. Komarov, A.F. Komarov, P. Tarkovsky, S.A. Fedotov, *Tech. Phys.* **64**, 106 (1994).
- [17] F.F. Komarov, A.F. Komarov, A.S. Petrov, *Mikroelektronika* **31**, 361 (2002).
- [18] C.W. Yuan, C.N. Boswell, S.J. Shin, C.Y. Ziao, J. Guzman, J.W. Ager, E.E. Haller, V.C. Chrzan, *Appl. Phys. Lett.* **95**, 083120 (2005).
- [19] Y. Ramaswamy, T.E. Haynes, C.W. White, W.J. Moberlychan, S. Roorda, M.J. Aziz, *Nano Lett.* **5**, 373 (2005).
- [20] Y. Yang, C. Zhang, Y. Song, J. Gou, Z. Zhang, Y. Meng, H. Zhang, Y. Ma, *Nucl. Instrum. Methods Phys. Res. B* **308**, 24 (2013).
- [21] A.V. Krasheninnikov, K. Norlund, *J. Appl. Phys.* **107**, 071301 (2010).
- [22] I. Lifshitz, V. Slyozov, *J. Phys. Chem. Solids* **19**, 35 (1961).
- [23] C. Wagner, *Zeitschrift für Elektrochemie* **65**, 581 (1961).
- [24] G. Mattei, P. Mazzoldi, H. Bernas, *Materials Science with Ion Beams*, Springer-Verlag, Berlin 2010.
- [25] M. Makhavikou, F. Komarov, I. Parkhomenko, L. Vlasukova, O. Milchanin, J. Žuk, E. Wendler, I. Romanov, O. Korolik, A. Togambayeva, *J. Surf. Coat. Technol.* **344**, 596 (2018).
- [26] M.A. Makhavikou, F.F. Komarov, O.V. Milchanin, L.A. Vlasukova, I.N. Parkhomenko, E. Wendler, J. Žuk, in: *Lecture Notes in Mechanical Engineering*, Springer Nature, 2019, p. 377.
- [27] A.F. Komarov, F.F. Komarov, O.V. Milchanin, L.A. Vlasukova, I.N. Parkhomenko, V.V. Mikhailov, M.A. Mokhovikov, S.A. Miskevich, *Tech. Phys.* **60**, 1335 (2015).
- [28] J.F. Ziegler, M.D. Ziegler, J.P. Biersack, *Nucl. Instrum. Methods Phys. Res. B* **268**, 1818 (2010).
- [29] M. Mayer, *AIP Conf. Proc.* **475**, 541 (1999).
- [30] F.F. Komarov, A.P. Novikov, A.F. Burenkov, *Ion Implantation*, Belarusian State University Press, Minsk 1994.